Dalton Transactions

PAPER

View Article Online
View Journal | View Issue

Cite this: *Dalton Trans.*, 2014, **43**, 2835

Synthesis and structural characterization of dioxomolybdenum and dioxotungsten hydroxamato complexes and their function in the protection of radiation induced DNA damage†

Shiv Shankar Paul,[a] Md. Selim,[a] Abhijit Saha[b] and Kalyan K. Mukherjea*[a]

Received 4th September 2013,
Accepted 8th November 2013

DOI: 10.1039/c3dt52434e

www.rsc.org/dalton

The synthesis and structural characterization of two novel dioxomolybdenum(VI) (**1**) and dioxotungsten(VI) (**2**) complexes with 2-phenylacetylhydroxamic acid (PAHH) $[M(O)_2(PAH)_2]$ [M = Mo, W] have been accomplished. The dioxomolybdenum(VI) and dioxotungsten(VI) moiety is coordinated by the hydroxamate group (–$CONHO^-$) of the 2-phenylacetylhydroxamate (PAH) ligand in a bi-dentate fashion. In both the complexes the PAHH ligand is coordinated through oxygen atoms forming a five membered chelate. The hydrogen atom of N–H of the hydroxamate group is engaged in intermolecular H-bonding with the carbonyl oxygen of another coordinated hydroxamate ligand, thereby forming an extended 1D chain. The ligand as well as both the complexes exhibit the ability to protect from radiation induced damage both in CTDNA as well as in pUC19 plasmid DNA. As the damage to DNA is caused by the radicals generated during radiolysis, its scavenging imparts protection from the damage to DNA. To understand the mechanism of protection, binding affinities of the ligand and the complex with DNA were determined using absorption and emission spectral studies and viscosity measurements, whereby the results indicate that both the complexes and the hydroxamate ligand interact with calf thymus DNA in the minor groove. The intrinsic binding constants, obtained from UV–vis studies, are 7.2×10^3 M^{-1}, 5.2×10^4 M^{-1} and 1.2×10^4 M^{-1} for the ligand and complexes **1** and **2** respectively. The Stern–Volmer quenching constants obtained from a luminescence study for both the complexes are 5.6×10^4 M^{-1} and 1.6×10^4 M^{-1} respectively. The dioxomolybdenum(VI) complex is found to be a more potent radioprotector compared to the dioxotungsten(VI) complex and the ligand. Radical scavenging chemical studies suggest that the complexes have a greater ability to scavenge both the hydroxyl as well as the superoxide radicals compared to the ligand. The free radical scavenging ability of the ligand and the complexes was further established by EPR spectroscopy using a stable free radical, the DPPH, as a probe. The experimental results of DNA binding are further supported by molecular docking studies.

1. Introduction

Radiotherapy is commonly employed as a part of the management of a wide variety of malignancies and is frequently used to achieve local or regional control of it either alone or in combination with other modalities such as chemotherapy or surgery. It is estimated that half of all cancer patients will receive radiotherapy by way of their treatment for cancer.[1] Irradiation of non-cancerous "normal" tissues during the course of therapeutic radiation can result in a range of side effects including self-limited acute toxicities, mild chronic symptoms, or severe organ dysfunction.[2] Efforts to reduce the toxicities associated with therapeutic radiation have centred both on technological improvements in radiation delivery as well as improvements in chemical modifiers to control radiation induced injury.[3] An alternative mechanism to reduce

[a]*Department of Chemistry, Jadavpur University, Calcutta, Kolkata-700032, India. E-mail: k_mukherjea@yahoo.com; Fax: +(91) (33)24146223; Tel: Cell phone: +(91) 9831129321*

[b]*UGC-DAE-CSR, Kolkata Centre, III/LB-8, Bidhannagar, Kolkata 700098, India*

†Electronic supplementary information (ESI) available: The ORTEP view and crystal packing structure for complex **2** [Fig. S1(a) and (b)], the absorption spectra of the ligand and the complexes **1** and **2** in the absence and presence of increasing amounts of DNA [Fig. S2(a)–(c)], emission spectra of complex **2** in the presence of increasing amounts of DNA [Fig. S3], viscometric studies of the ligand, Mo-complex and W-complex [Fig. S4], fluorescence spectra of the EB-DNA with different doses of radiation at a dose rate of 69.3 Gy min^{-1} for 5–60 min [Fig. S5], gel electrophoresis study of pUC19 DNA in the presence of the ligand, complexes **1** and **2** [Fig. S6], protection of the plasmid pUC19 DNA at 20 Gy with different doses of the ligand, complex **1** and complex **2** on gamma-radiation induced strand breaks [Fig. S7] and DPPH scavenging activity of complexes **1** and **2**. CCDC 795762 and 878566 for complexes **1** and **2** respectively. For ESI and crystallographic data in CIF or other electronic format see DOI: 10.1039/c3dt52434e

damage to normal tissues is the use of radiation modifiers/protectors, present prior to or shortly after radiation exposure to alter the response of normal tissues to irradiation.[4] This approach has also been viewed as an attractive countermeasure for possible nuclear/radiological terrorism. So far, a number of compounds have been reported to have radiation protective properties, only amifostine is currently in clinical use.[5] From the above facts it becomes apparent that development of radioprotector molecules is highly warranted to take care of the radiation induced damage to normal tissues occurring during radiotherapy. Although the preparation of metal based radioprotectors[6] is of prime importance as they can prevent normal cells from death during radiotherapy of cancer, the prevalence of metal based radioprotectors is rare. The metal complexes can interact covalently and non-covalently with double helical DNA that include three types of binding modes, *viz.* intercalative, covalent binding and external electrostatic binding, and among the different types of molecules, the metallointercalators have received particular attention.[7]

Amongst the metals, molybdenum, the 4d transition element, has been known to have wide biological functions for life on earth. The physiologically active oxidation states of molybdenum are +4, +5 and +6 while they are commonly co-ordinated to the proteins.[8,9] The essential role of molybdenum in biology has been known for decades and molybdoenzymes are ubiquitous, but it is only recently that the biological role of tungsten has been established in prokaryotes.[9] Different types of tungstoenzymes have been purified: formate dehydrogenase, formyl methanofuran dehydrogenase, acetylene hydratase, and a class of phylogenetically related oxidoreductases that catalyze the reversible oxidation of aldehydes.[9]

On the other hand, the chemistry and biochemistry of hydroxamic acid and its derivatives have attracted considerable attention, due to their pharmacological, toxicological and pathological properties. Hydroxamic acid derivatives generally have low toxicities with a wide spectrum of activities in all types of biological systems: they act as growth factors, food additives, tumor inhibitors, antimicrobial agents, antitubercular, antileukemic agents, key pharmacophores[10] in many important chemotherapeutic agents, pigments and cell-division factors. Several of them have advanced into human clinical trials as pharmaceutical drugs for the treatment of several diseases.[11] They have also been employed as insecticides, antimicrobials, and plant growth regulators[11] and are also used industrially as antioxidants, inhibitors of corrosion, for the extraction of toxic elements, and as a means of flotation of minerals. The exploration of the chemistry of the hydroxamic acid derivatives relevant to applications in the biomedical sciences has been focussed on.[11] So, in the present study, the synthesis and characterization of the potential metal complex with the biologically relevant ligand, the hydroxamate, have been undertaken for its possible application as a radioprotector. The ligand was chosen taking into account the availability of oxygen and nitrogen atoms that can establish hydrogen bonds with the DNA, and finally, the possibility that the metal complex can interact with the DNA in the groove. The DNA binding of the complex has been studied with CT DNA whereas the protection of DNA damage from radiation is demonstrated with both CT DNA and plasmid DNA. The radioprotecting ability of the complex and the ligand has been established by fluorescence emission spectroscopy as well as gel electrophoresis measurements in appropriate cases. The results of the above studies suggest that the synthetic molecules used are capable of providing protection from radiation induced DNA damage very efficiently.

2. Results & discussion

2.1. Synthetic aspects and spectroscopic characterization of the complexes

The 2-phenylacetylhydroxamate (O, O donor) ligand was synthesized by a literature method.[12] The molybdenum and tungsten-dioxo complexes were synthesized by the reaction of aqueous $MO_3{\cdot}H_2O$ [M = Mo, W] solution with 30% H_2O_2 resulting in a non-isolable peroxo species; this on reaction with the methanolic solution of PAHH ligand afforded the dioxo $[M(O)_2(PAH)_2]$ [M = Mo, W] as a solid residue. The molybdenum complex is designated as complex **1** while the corresponding tungsten complex is designated as complex **2**. The complexes are soluble in methanol, acetonitrile, and highly polar solvents like DMF and DMSO and behave as non-electrolytes. Complexes **1** and **2** are also diamagnetic at 298 K.

The IR spectra of the dioxo compounds are known to show two strong bands[13] centred around 907–914 and 934–949 cm^{-1} attributable to the asymmetric and symmetric [M = O {M = Mo, W}] stretches, respectively, in the *cis*-dioxo moieties. In the present case the ν(Mo═O) and ν(W═O) vibrations in the complexes appear at 905, 960 cm^{-1} and 915, 967 cm^{-1}, respectively, which are in agreement with earlier observations.[13] In free PAHH (*N*-phenylacetyl hydroxamic acid), the ν(C═O) vibration occurs at 1634 cm^{-1}, while after coordination with metals [Mo(VI) and W(VI)], the ν(C═O) of co-ordinated PAH^- appears at 1597 cm^{-1} and 1605 cm^{-1} for complexes **1** and **2** respectively. The shifting of the ν(C═O) absorption band to a lower energy region indicates the decrease in C═O bond order due to drainage of electron density from the carbonyl oxygen to the metal [Mo & W] centre.

The electronic spectrum of the free ligand shows a broad peak at 249 nm which corresponds to intraligand transition. There appear bands at 207 nm and 210 nm in complex **1** and complex **2** respectively which are assigned as the intraligand $\pi\rightarrow\pi^*$ transition of the aromatic ring and another broad band for both the complexes from 240 to 305 nm is due to $n\rightarrow\pi^*$ of the C═O functional group of the coordinated ligand. From the NMR study it was confirmed that complexes **1** & **2** as well as the ligand are stable in solution phase. In both complexes **1** and **2** the hydroxamate –OH is deprotonated, which is characterized by the disappearance of the –OH proton signal at δ 4.8; this suggests that the ligand behaves as a mono

anionic O, O donor centre. So, Mo and W metal centres are in the +VI oxidation state which is further supported by the diamagnetic nature of the complexes.

2.2. Crystal structure

The molecular structures of both complexes **1** and **2** have been determined by single crystal X-ray diffraction analysis, and the data are presented in Table 1 whereas the selected bond lengths and bond angles are listed in Table 2. Complexes **1** and **2** crystallize in the monoclinic *C*2/*c* space group, and a representative ORTEP view of asymmetric units of complex **1** is shown in Fig. 1(a). The complexes exhibit distorted octahedral geometry whereas the coordinating sites are occupied by two dioxo ligands in *cis* arrangement and the remaining four sites are coordinated by two oxygen atoms of each of the two participating (–CONHO$^-$) ligand moieties. An imposed C_2 axis bisects the O(1)–M–O(1A) [M = Mo, W] angle, application of which generates the full complex. The M═O [Mo and W] bond lengths for (M–O1) and (M–O1A) were 1.689(14) Å for complex **1** and 1.705(3) Å for complex **2**, which are in the typical range for group 6 metal oxo bonds.[14] The M–O2 (carbonyl oxygen) bond lengths in complex **1** are 2.245(12) Å and 2.242(2) Å in complex **2**, while the M–O3 (N–O) bond lengths are 1.990(11) Å in complex **1** and 1.983(19) Å in complex **2** which are comparable to other reported hydroxamato complexes available in the literature.[15,16] The O, O coordination of chelated hydroxamate ligand fragments (O2, O3, C1 and N1), excluding the phenyl group, is essentially planar and is approximately orthogonal to another hydroxamato group of the ligand having the same coordination. The dihedral angle between the two planes is 92.86(1) in **1** and 92.79(1) in **2**. The bond distances between the metal and the O, O donor hydroxamato (–CONHO$^-$) moiety of the ligand are in agreement with the single bond reported elsewhere.[17] The crystal packing arrangement in the structure exhibits weak intermolecular N–H···O hydrogen bond interaction between N–H of the hydroxamate group and the carbonyl oxygen of another coordinated hydroxamate ligand, which leads to the formation of a one dimensional chain (a representative packing diagram is shown in Fig. 1(b)). The relevant hydrogen bonding parameters are shown in Table 3. The ORTEP view and packing pattern of complex **2** are shown in ESI Fig. S1(a) and (b).†

Table 1 Crystal data and structure refinement parameters of the complex

Parameters	Complex **1**	Complex **2**
Empirical formula	$C_{16}H_{16}N_2O_6Mo$	$C_{16}H_{16}N_2O_6W$
M_r	428.25	516.15
T/K	293(2)	293(2)
λ/Å	0.71073	0.71073
Crystal system	Monoclinic	Monoclinic
Space group	*C*2/*c*	*C*2/*c*
Unit cell dimensions		
a/Å	17.4688(4)	17.4365(16)
b/Å	10.5106(4)	10.5304(16)
c/Å	9.4600(2)	9.4876(10)
α/°	90.00	90
β/°	103.987(2)	104.276(2)
γ/°	90.00	90
V/Å^3	1685.43(8)	1688.3(3)
Z, D_c/g cm^{-3}	4, 1.688	4, 2.031
F(000)	864	992
Crystal size/mm	0.05 × 0.07 × 0.15	0.04 × 0.08 × 0.15
θ Range for data collection (°)	2.28, 27.64	2.28, 25.0
Reflection	12 587	5789
Independent reflections (R_{int})	1953(0.019)	1489(0.026)
Completeness to $\theta = \theta_{max}$ (%)	99.1	100
Refinement method	Full-matrix-least-squares on F^2	
Data/restraints/parameters	1953/0/114	1489/0/114
Goodness-of-fit on F^2	1.109	1.074
Final R indices [$I > 2\sigma(I)$]	R_1 = 0.0203	R_1 = 0.0174
	wR_2 = 0.0535	wR_2 = 0.0446
R indices (all data)	R_1 = 0.0218	R_1 = 0.0182
	wR_2 = 0.0544	wR_2 = 0.0450
Largest diff. peak, hole/Å^{-3}	−0.375, 0.232	−0.412, 0.491

Table 2 Selected bond lengths (Å) and bond angles (°) of the complex

Bond lengths (Å)			
$[Mo(O)_2(PAH)_2]$ (**1**)		$[W(O)_2(PAH)_2]$ (**2**)	
Mo–O(1)	1.689(14)	W–O(1)	1.705(3)
Mo–O(2)	1.990(12)	W–O(2)	1.982(2)
Mo–O(3)	2.245(12)	W–O(3)	2.242(2)
O(3)–C(1)	1.267(18)	O(3)–C(1)	1.270(3)
O(2)–N(1)	1.366(19)	O(2)–N(1)	1.368(3)
N(1)–C(1)	1.298(2)	N(1)–C(1)	1.298(4)
N(1)–H(1)	0.860	N(1)–H(1)	0.860
Bond angles (°)			
O(1)–Mo–O(2)	105.78(7)	O(1)–W–O(2)	90.90(11)
O(1)–Mo–O(3)	89.59(6)	O(1)–W–O(3)	160.72(10)
O(1)–Mo–O(1a)	105.53(8)	O(1)–W–O(1a)	105.52(12)
O(1)–Mo–O(2a)	90.68(7)	O(1)–W–O(2a)	105.46(11)
O(2)–Mo–O(3)	73.45(4)	O(2)–W–O(3)	73.56(8)
O(2)–Mo–O(2a)	152.87(5)	O(2)–W–O(2a)	153.02(9)
O(2)–Mo–O(3a)	85.51(4)	O(2)–W–O(3a)	85.41(8)
O(3)–Mo–O(3a)	78.55(5)	O(3)–W–O(3a)	77.78(8)
Mo–O(3)–C(1)	112.63(10)	W–O(3)–C(1)	112.73(18)
O(1)–Mo–O(3a)	160.73(6)	O(1)–W–O(3a)	160.72(10)
Mo–O(2)–N(1)	117.18(9)	W–O(2)–N(1)	117.11(17)
C1–N1–H1	121.00	C1–N1–H1	121.00
O2–N1–H1A	121.00	O2–N1–H1	121.00
O3–C1–C2	123.56(15)	O3–C1–C2	123.3(3)
O3–C1–N1	117.49(15)	O3–C1–N1	117.0(3)
N1–C1–C2	118.94(14)	N1–C1–C2	119.7(3)

2.3. DNA binding studies

The present study is directed towards the development of synthetic molecules capable of providing protection from radiation induced DNA damage. This protection can be imparted primarily through DNA binding and scavenging of radiolysed radicals. So, establishment of the ability of protection of the double stranded DNA damage from a given molecule demands a thorough study on the interaction of DNA with the potential protector molecule. Hence, the binding of DNA with the synthetic molecules has been studied, the results of which are being presented herein.

2.3.1. Electronic absorption spectral studies. Electronic absorption spectroscopy is one of the simplest techniques usually utilized to examine the binding of metal complexes with DNA. The electronic spectra of both complexes **1** & **2** and the ligand in the presence and absence of DNA were

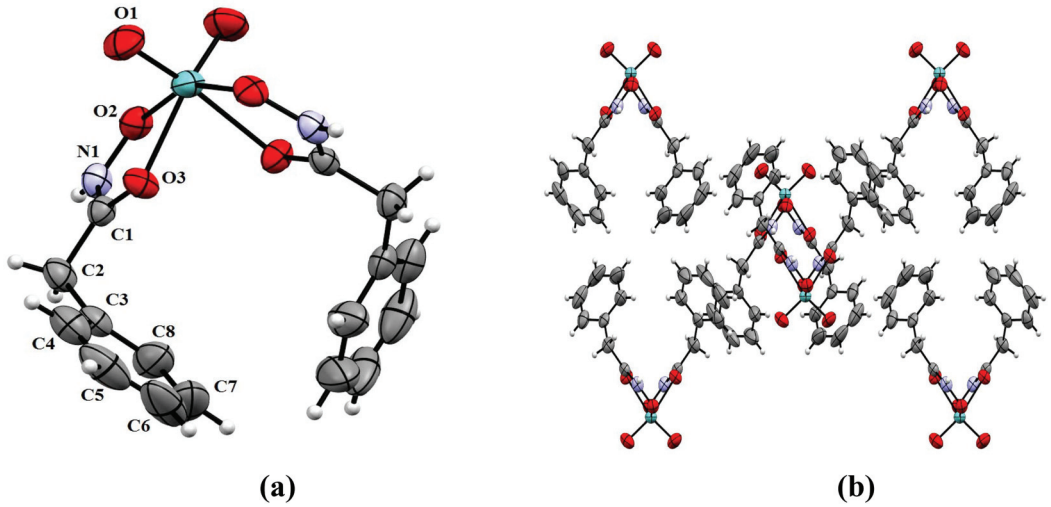

Fig. 1 (a) ORTEP representation of the X-ray crystal structure of complex **1**, with all non-hydrogen atoms shown as 50% thermal ellipsoids. (b) Crystal packing of complex **1**.

Table 3 Relevant hydrogen bonds in the complex

D–H···A	*d*(D–H)	*d*(H···A)	*d*(D···A)	∠(DHA)
$[Mo(O)_2(PAH)_2]$ (1)				
N(1)–H(1)···O(3)$^{(i)}$	0.86	2.07	2.853(17)	151
$[W(O)_2(PAH)_2]$ (2)				
N(1)–H(1) ···O(3)$^{(ii)}$	0.86	2.09	2.864(3)	150

(i) x, $1 - y$, $-1/2 + z$; (ii) x, $-y$, $-1/2 + z$.

monitored. Upon the addition of incremental amounts of DNA, increases in the absorptivity and red shift (2 nm) of the ligand and both complexes **1** & **2** were observed. Hoechst 33258 family groove binders also exhibit red shifts of absorption bands when they bind to the grooves of a DNA helix. A plot of $[DNA]/(\varepsilon_a - \varepsilon_f)$ *versus* [DNA] gives the binding constants which were calculated to be $(5.2 \pm 0.2) \times 10^4$ M^{-1} for DNA-complex **1**, $(1.2 \pm 0.2) \times 10^4$ M^{-1} for DNA-complex **2** and $(7.2 \pm 0.2) \times 10^3$ M^{-1} for DNA-ligand, respectively, which indicates that both complexes **1** & **2** and the ligand approach DNA through the groove.[18] The corresponding results of absorbance spectral studies are provided as ESI [Fig. S2(a)–(c)†].

2.3.2. Emission titrations. The PAHH ligand does not show any emission, but when it is coordinated to the molybdenum or tungsten, it shows emission. $[Mo(O)_2(PAH)_2]$, complex **1**, on excitation at 250 nm exhibits emission at 307.5 nm, whereas $[W(O)_2(PAH)_2]$, complex **2**, on excitation at 270 nm exhibits emission at 290 nm, so these are intrinsic fluorophores.

The emission intensities of complexes **1** and **2** decrease gradually on progressive addition of CT-DNA [Fig. 2 & ESI Fig. S3†], which suggests binding of DNA with both complexes **1** and **2**. The fluorescence intensity becomes constant at a high concentration of DNA, which indicates that the binding has reached saturation. The fluorescence quenching constants (K_{SV}) evaluated using the Stern–Volmer equation were found to

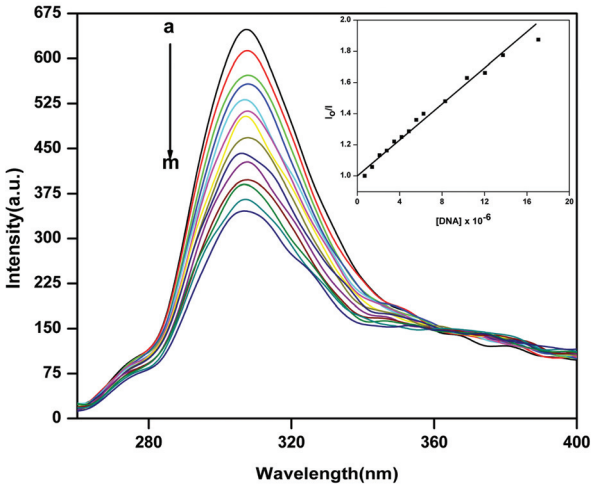

Fig. 2 Emission spectra of complex **1** in the presence of increasing amounts of DNA (a) 0.0 μM, (b) 10 μM, (c) 20 μM, (d) 40 μM, (e) 60 μM, (f) 80 μM, (g) 100 μM, (h) 110 μM, (i) 120 μM, (j) 130 μM, (k) 150 μM, (l) 180 μM and (m) 200 μM. (Inset: Stern–Volmer plot for MoP.)

be 5.6×10^4 M^{-1} and 1.6×10^4 M^{-1} for complexes **1** and **2** respectively at 25 °C [inset in Fig. 2 & ESI Fig. S3†]. The linear Stern–Volmer plots with the intercept of 1.0 for both complexes **1** and **2** indicate that only one type of quenching process occurs, *i.e.*, static quenching in both the cases.

The results were further analysed using eqn (3) to get the required parameter P, which was determined either by measurement of the fluorescence emission of a given quantity of complex **1** or **2** in the presence and absence of a large excess of DNA or by the addition of DNA to a fixed amount of complex **1** or **2** until no further change in fluorescence emission was observed. A value of $P = 0.05$ was obtained regardless of the protocol and was used for further calculations. These experimental data are fitted to the neighbour exclusion model[19] (*vide* eqn (3)). The best fit to the

experimental data provides an exclusion parameter, n = 3.5 and 2 base pairs for both complexes **1** and **2**, while the intrinsic binding constants were found to be $K_i = 0.8 \times 10^5$ M^{-1} and 4.8×10^4 M^{-1} for complexes **1** and **2** respectively. The uncertainty in these parameters is roughly 15%. The number of binding sites is obtained from the *x*-intercept of the Scatchard plot. This phenomenon can be accounted for with the neighbour exclusion model,[19] which holds that the binding of a small molecule to one site influences the binding of subsequent molecules, and the subsequent molecules are excluded from binding at nearby sites by either physical blockage or steric alterations in DNA.

2.3.3. Viscometric studies. Hydrodynamic measurement, mainly viscosity, is a sensitive technique to determine the DNA binding mode. The relative viscosity of CT-DNA solution is known to increase on intercalative binding of substrates, because the insertion of intercalators causes the base pairs of the DNA to get apart and thus causes a lengthening of the DNA helix. On the other hand, agents bound to DNA through a groove do not alter the relative viscosity of DNA, and the partial or non-classical intercalation of ligands may bend or kink the DNA helix, thereby decreasing its effective length and subsequently viscosity.[20] The values of relative specific viscosities of DNA in the absence and presence of complexes **1** & **2** and the ligand are plotted against [complex]/[DNA]. It is observed that the addition of either the complex **1** or **2** or the ligand to the CTDNA solution shows neither any significant increase nor any significant decrease in the viscosity of the CTDNA, thereby clearly demonstrating the non-intercalative binding of CTDNA by the present complexes **1** & **2** as well as the ligand; on the other hand, it hints at groove binding[21] [ESI Fig. S4†].

2.4. Radiation induced DNA damage and protection from it

2.4.1. Fluorimetric estimation of radiation induced damage in CT DNA. The fluorimetric assessment of radiation induced DNA damage was carried out using ethidium bromide (EB) as a probe, which has very feeble emission intensity in the aqueous medium. However, the emission intensity of EB is much enhanced in the presence of DNA due to its strong intercalation between the adjacent DNA base pairs. If radiation induces damage to the DNA double helix, the bound EB will be finding its way to come out of the base pairs in the aqueous environment again, or if EB is added immediately after irradiation of DNA, because of the damage in the double helix, relatively more EB will remain in aqueous solution, which will be reflected in a decrease in fluorescence intensity. This relative decrease in fluorescence intensity of EB bound to DNA proves that the damage in the DNA double helix is a function of dose of radiation. In the present case, irradiation of DNA with γ-rays causes a decrease in the fluorescence intensity of EB. The greater the dose of the radiation, the greater is the decrease in fluorescence intensity of EB. These dose–effect curves for gamma radiation induced DNA strand breaks are purely linear, and the estimation indicates a 68% DNA damage by the radiation at the present experimental set-up (ESI Fig. S5†).

2.4.2. Estimation of the protection from DNA damage by the fluorometric technique. The amount of retention of double stranded DNA after irradiation was calculated from dose–effect curves (ESI Fig. S5†). D_{50} (50% DNA remains unchanged) was calculated from the dose–response curve and the time required for it was also determined. After irradiating the DNA for 35 min, *i.e.*, at D_{50}, the fluorescence intensity of the EB bound DNA decreases sharply with respect to the control DNA, indicating radiation induced damage. For protecting the DNA from radiation induced damage, DNA was pretreated with different concentrations of either the ligand or the complex **1** or **2** in appropriate cases and then radiation was given, thereafter the emission intensity of EB was measured. It is observed that the fluorescence intensity of EB-DNA solution is increased with an increase in the concentration of either the ligand or the complexes **1** & **2**, the results of which are shown in Fig. 3(a)–(c). The concentration of the ligand and the complexes used is over the range of 0.4 μM to 20 μM, and it is observed that with the increase in concentration there occurs a gradual increase in the fluorescence intensity of EB bound to irradiated DNA. This indicates that the ligand as well as both the complexes impart protection to the CTDNA from the damage induced by radiation.

A plot of $(I - I_a)/(I_0 - I_a)$ *versus* [radioprotector]/[CT-DNA] has been made. This is shown as the inset in Fig. 3(a)–(c) where it is found that with the increase in the concentration of either the ligand or both complexes **1** and **2**, the damage caused by radiation to DNA is inhibited. Precisely, the percentage of protection imparted either by the ligand or by the Mo and W-complexes was evaluated to be 72, 87 and 80%, respectively. The protection from radiation induced CT DNA damage is very much pronounced in the case of the Mo-complex compared to the ligand and W-complex. The ligand imparts 72% protection from the damage; the Mo-complex is capable of imparting 87% protection whereas its counterpart, the W-complex, imparts 80% protection to the double stranded DNA. It may be mentioned here that the binding constant of the complexes is also higher than the ligand. Ionizing radiation on interaction with water in cells can produce reactive free radicals, such as hydroxyl radicals, hydrogen radicals, ROS, hydrogen peroxide and toxic substances, all of which can damage critical macromolecules. The elimination of the free radical species from the cell environment can inhibit the side effects induced by irradiation. Scavenging of the radiolysed radicals arising out of the irradiation of water molecules can confer protection to the cellular materials from radiation. In the present case, as the ligand and both complexes **1** and **2** are groove binders, they are capable of protecting the double stranded DNA from radiation induced damage. But the abilities of protection of the ligand and complexes **1** and **2** are different. Even at a low concentration, the Mo-complex (8 μM) is able to impart about 80% protection from radiation induced damage to DNA compared to 72% for the W-complex at the same concentration. Although with the increase in concentration the ligand and both complexes **1** and **2** show enhanced protection, in the case of the Mo-complex it is more pronounced; precisely, at 15 μM

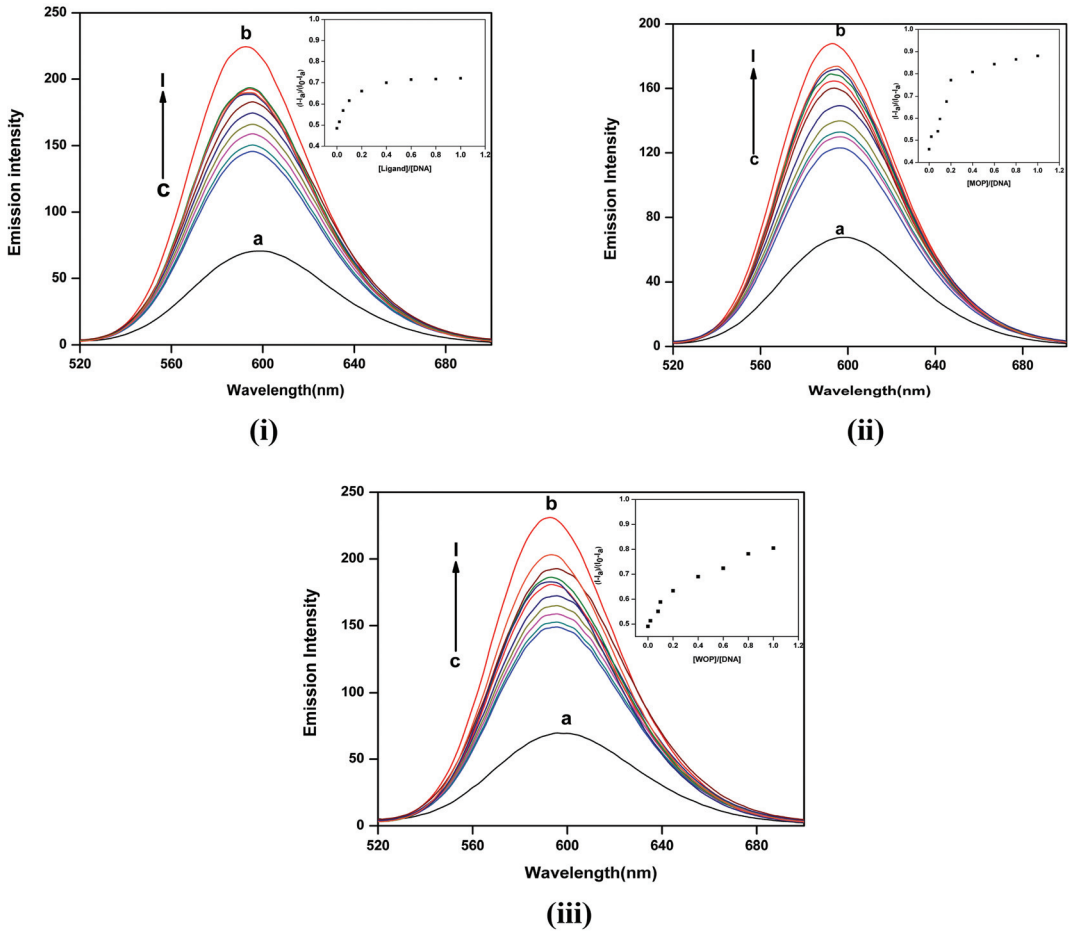

Fig. 3 Fluorescence emission spectra of the EB-DNA in presence of increasing amounts of (i) ligand, (ii) MoP, (iii) WoP after 35 min of gamma-irradiation [EB] = 30.0 μM for (a), [EB] = 30.0 μM + [DNA] = 20.0 μM (unirradiated) for (b); (c–l) [Ligand or Complex]/[DNA]: 0–1 (irradiated). (Inset: Plot of $(I - I_a)/(I_0 - I_a)$ *versus* [ligand or Complex]/[DNA].)

concentration, the ligand, the W-complex and the Mo-complex impart 72%, 80% and 87% protection respectively. So, even at a low concentration, complex **1** responds well to the protection of damaged DNA from radiation, compared to the ligand and complex **2**. The potentiality of metal complexes to protect the damaged DNA is greater than the ligand, due to chelation of the ligand to the metal centre. Therefore, complexes **1** and **2** have a greater ability to protect than the ligand.

2.4.3. The role of the ligand and complexes 1 and 2 in the protection from gamma-radiation induced strand breaks in plasmid pUC19 DNA. The gel electrophoresis studies with pUC19 plasmid DNA show that neither the ligand nor the complex alone does induce any nicking in the plasmid pUC19 DNA (ESI Fig. S6†) at different concentrations of 1.0 and 2.0 mM. Exposure of the plasmid DNA to gamma-radiation at different doses leads to strand breaks resulting in relaxation of plasmid DNA from a supercoiled (SC) form to a nicked coil (NC) form.[22] The plasmid DNA is subjected to doses of radiation of 20 Gy and 25 Gy, which cause damage to the supercoiled plasmid DNA. When pUC19 DNA is subjected to gamma-radiation induced strand breaks, 50% and 60% of the SC form plasmid DNA got converted into open circular form at doses of 20 & 25 Gy, respectively, as is evident from the figures (ESI Fig. S7† & Fig. 4, lane 2). The treatment of radiation induced damaged pUC19 DNA with different concentrations of either complexes **1** and **2** or the ligand shows significant protection from the damage. The damage caused by radiation is mainly due to the formation of radicals. Complexes **1**, **2** and

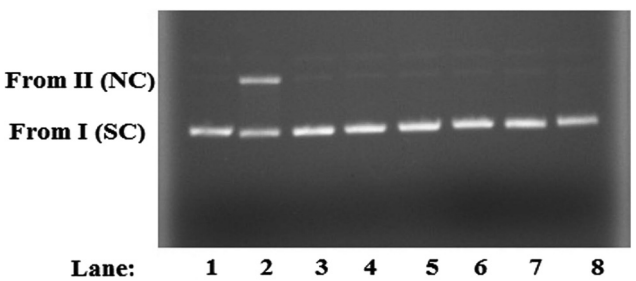

Fig. 4 Protection of plasmid pUC19 DNA at 25 Gy with different doses of ligand, complex **1** and complex **2** on gamma-radiation induced strand breaks.

Table 4 Extent of DNA SC pUC19 protection by the ligand and the complex

Lane no.	Reaction condition	Form I (% SC)	Form II (% NC)
1	DNA CONTROL (No radiation)	96	4

		20 Gy		25 Gy	
Radiation dose		Form I (% SC)	Form II (% NC)	Form I (% SC)	Form II (% NC)
2	DNA irradiated	50	50	40	60
3	DNA + 1 mM (0.015 μg) ligand	62	38	70	30
4	DNA + 1 mM (0.0428 μg) MOP complex	73	27	78	22
5	DNA + 1 mM (0.0516 μg) WOP complex	68	32	72	28
6	DNA + 2 mM (0.030 μg) Ligand	80	20	75	25
7	DNA + 2 mM (0.0956 μg) MOP complex	95	5	85	15
8	DNA + 2 mM (0.1032 μg) WOP complex	87	13	76	24

the ligand might be able to eliminate the radicals that cause damage to the supercoiled DNA. The results of this experiment are presented in Table 4. The ligand and complexes **1** and **2** could afford protection from radiation induced damage to the plasmid DNA; at a concentration of 2.0 mM of either the ligand or complex **1** or **2**, the ligand imparts 80% and 75% protection at doses of 20 and 25 Gy respectively, whereas complex **1** imparts 95% and 85% protection, and for complex **2** the protection is 87% and 76% at doses of 20 and 25 Gy, respectively. Thus, it is evident that the ligand as well as the complexes could offer significant protection to DNA against gamma-radiation induced damage *in vitro* by reducing the formation of strand breaks.

2.5. Mechanism of protection from radiation induced DNA damage

Radiation induced DNA damage is mainly caused by the splitting of water to generate reactive oxygen species (ROS) during radiolysis.[23] ROS are mainly free radicals. Scavenging of the free radicals which are generated during radiolysis is of prime importance as these cause damage to DNA. So, for protection from DNA damage from radiation, it is important to remove these free radicals, *i.e.* ROS ($OH^{\bullet}$ hydroxyl radicals and superoxide anion radicals), from the system.

As the ligand as well as the complexes exhibit protection from radiation induced DNA damage, it is considered worthwhile to study other potential aspects, such as radical scavenging activity by the ligand or complexes **1** and **2** to understand the mechanism of action. The radical scavenging activities of the ligand and complexes **1** & **2** along with the standards have been examined. The standards used were mannitol and vitamin C for hydroxyl radicals ($OH^{\bullet}$), and quercetin for superoxide anion radicals ($O^{2-\bullet}$).

2.5.1. Hydroxyl radical scavenging activity. The hydroxyl radicals were generated through a Fenton-type reaction, in which the degradation of safranin was measured in a Fe(II)–EDTA–H_2O_2 reaction mixture. The ability of the complexes **1**, **2** and the ligand to scavenge hydroxyl radicals was compared with those of the well-known natural antioxidants[23] mannitol and vitamin C. The 50% inhibitory concentration (IC_{50}) values of mannitol and vitamin C are about 1×10^{-3} and 0.9×10^{-3} M respectively. According to the scavenging experiments, the IC_{50} values of the ligand and the complexes **1** & **2** are found to be 1×10^{-4} M, 6.5×10^{-5} M, and 1.2×10^{-5} M, respectively, which implies that the complexes **1** and **2** exhibit better scavenging activity than mannitol and vitamin C.[24] Moreover, the ligand and both the complexes **1** and **2** are also capable of scavenging the radiolysed radicals.

2.5.2. Superoxide radicals ($O_2^{-\bullet}$) scavenging activity. The ability to reduce NBT by superoxide radicals generated from dissolved oxygen by PMS-NADH coupling[25] can be measured by a decrease in the absorbance of the reaction mixture at 560 nm. The absorbance at 560 nm is affected when the control solution is treated with different concentrations of the ligand as well as complexes **1** and **2**. Complexes **1**, **2** and the ligand show a gradual decrease in the absorbance at 560 nm, indicating their ability to scavenge superoxide radicals from the reaction mixture. The ability of the ligand and the complexes **1**, **2** to scavenge superoxide radicals from the solution was found to be higher than that of the standard. The inhibitory concentration (IC_{50}) value for the standard quercetin is about 7×10^{-3} M, while the IC_{50} values for the corresponding ligand and the complexes were found to be 3.6×10^{-4} M, 4.2×10^{-5} M and 0.9×10^{-5} M, respectively.

2.5.3. Assessment of the scavenging of DPPH

2.5.3.1. Assessment of the scavenging of DPPH by EPR spectroscopy. The elimination of radicals from the solution by scavenging will protect other molecules of the solution from radiation induced damage, if any entity capable of scavenging free radicals is used during radiolysis. The molecules which we have used to protect from DNA damage have been shown to scavenge free radicals from the system. So, to establish the radical scavenging activity of our molecules in a more sophisticated way, EPR spectroscopy was used. The model of scavenging the stable radical, DPPH, is a widely used method[26] to evaluate antioxidant capacities of natural and synthetic products. The EPR signal of DPPH was used to monitor the free radical scavenging activity of our complex and the ligand. The EPR spectra of the methanolic solutions of DPPH were taken. This

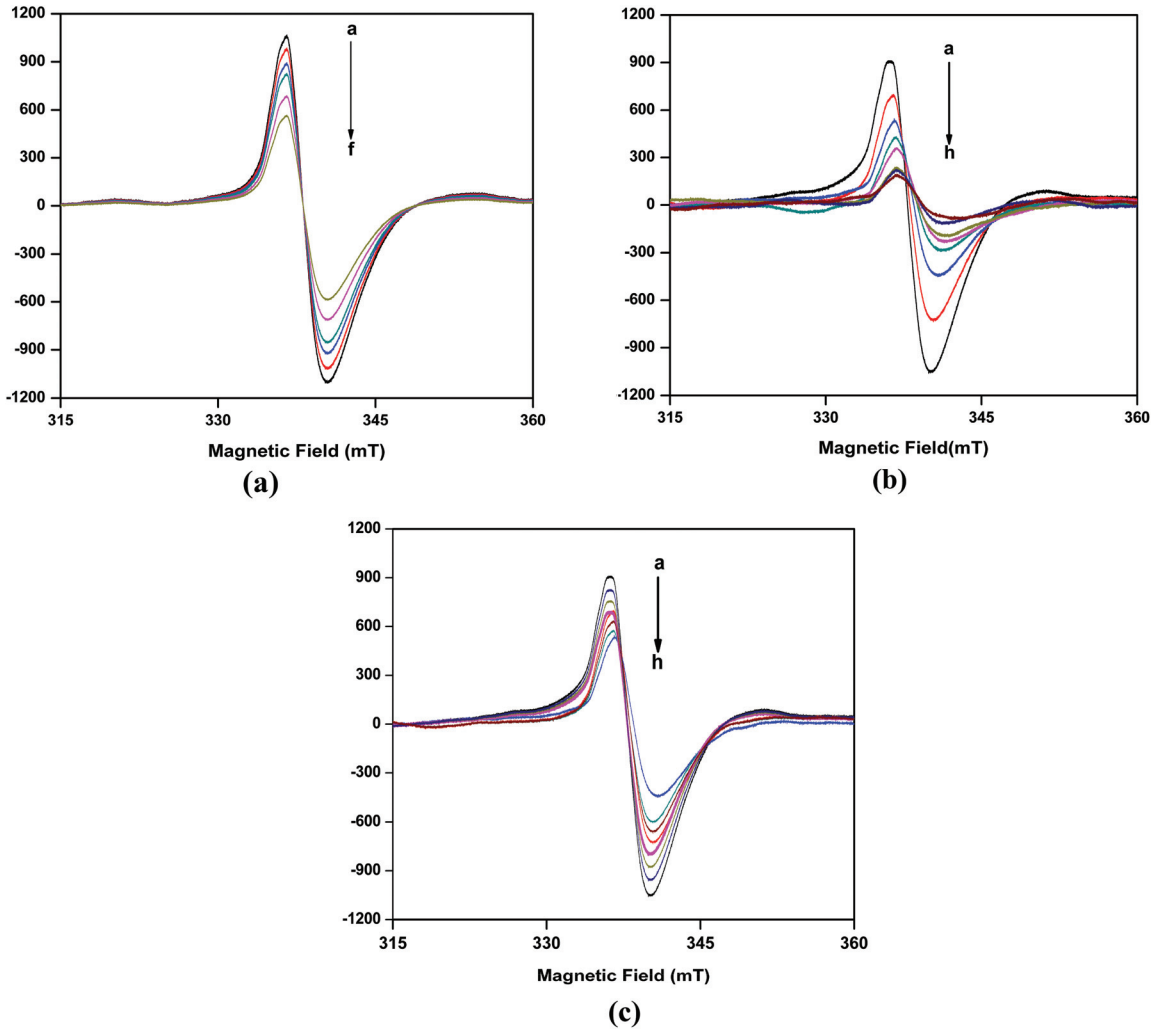

Fig. 5 (a) EPR spectra of DPPH (60 mM) with different concentrations of ligand in methanol solution (a–f: 0–60 mM). (b) EPR spectra of DPPH (60 mM) with different concentrations of complex **1** in methanol solution (a–h: 0–60 mM). (c) EPR spectra of DPPH (60 mM) with different concentrations of complex **2** in methanol solution (a–h: 0–60 mM).

DPPH was treated with incremental amounts of either the ligand [Fig. 5(a)] or the complexes **1** and **2** [Fig. 5(b) and (c)], and EPR was taken under identical conditions. Although it is found that both the complexes and the ligand can induce scavenging of free radicals of DPPH, the effect is more pronounced in the case of complex **1** than complex **2** and the ligand. This has also been exhibited in the actual DNA damage protection experimental results, where complex **1** has been found to impart greater protection from damage than complex **2** and the ligand. So, this experiment unequivocally supports our observation of the ability of protection from radiation induced DNA damage both by complexes **1**, **2** and the ligand.

2.5.3.2. Assessment of the scavenging of DPPH by electronic absorbance spectroscopy. The DPPH free radical scavenging property of the ligand and complexes **1** and **2** was investigated by electronic absorbance spectroscopy using DPPH as a stable free radical.[27] The radical scavenging was monitored at

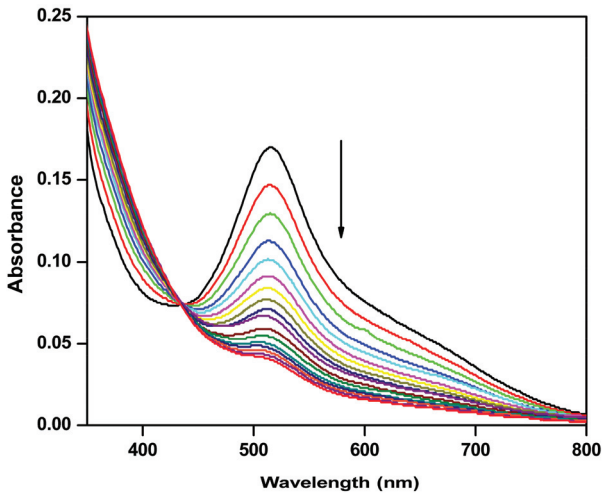

Fig. 6 Changes in the UV-vis spectrum of DPPH (0.1 μM) in the presence of MoP (complex **1**) (0–0.06 μM) in MeOH.

517 nm at different concentrations of the ligand and complexes **1** & **2**. The ability of the ligand and complexes **1**, **2** [Fig. 6 and ESI Fig. S8†] to scavenge DPPH free radicals from the solution was found to be higher than that of the standard. The inhibitory concentration (IC_{50}) value for the standard vitamin C is about 0.9×10^{-3} M, while the IC_{50} values for the corresponding ligand and the complex were found to be 1.6×10^{-4} M, 1.6×10^{-5} M and 2.8×10^{-5} M respectively. This study also supports the scavenging of free radical DPPH from the solution by the ligand and both the complexes **1** & **2**. This is done probably by the adduct formation.

Thus, from the scavenging experiments, it can be concluded that both the complexes **1** and **2** show greater scavenging activity compared to the ligand; this is due to the chelation of ligands with the central metal atom.[28] The lower IC_{50} values observed in radical scavenging assays did demonstrate that complexes **1**, **2** and the ligand have strong potentiality to be applied as scavengers to eliminate the radicals generated by radiolysis.

2.6. Molecular docking

2.6.1. Molecular docking investigation on the interaction of DNA with the ligand and complexes 1 & 2. The molecular docking technique is an attractive scaffold to understand the drug–DNA interactions for rational drug design and discovery, as well as to establish the mechanism of action of the reactants by placing a small molecule into the binding site of the target specific region of the DNA, mainly in a non-covalent fashion. However, a covalent bond may also be formed between the reactants. Different structural properties lead to different binding modes; in fact one of the most important factors governing the binding mode is the molecular shape. The literature[29] reveals that the forces

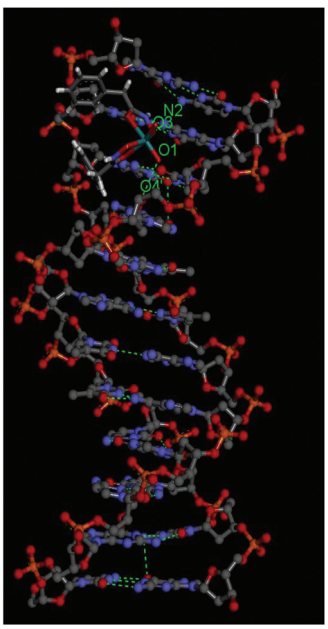

Fig. 7 Docked pose of Mop showing interaction with base pairs.

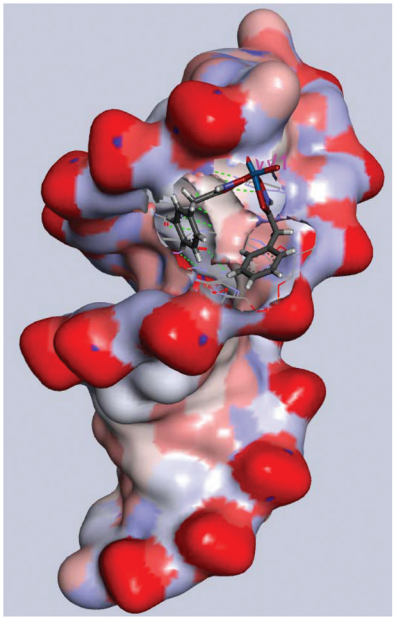

Fig. 8 Docked pose of Wop showing interaction with base pairs.

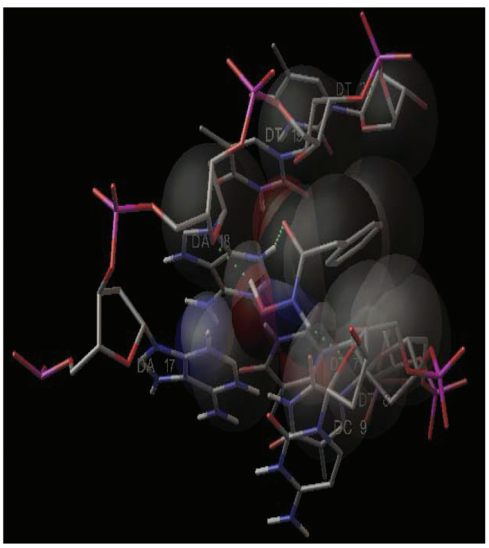

Fig. 9 Docked pose of ligand showing interaction with base pairs.

maintaining the stability of the DNA–intercalator complex include van der Waals forces, hydrogen bonding, hydrophobic charge transfer and electrostatic complementarity. In our experiment, the ligand and the complexes **1** & **2** were successively docked with the DNA duplex of the sequence d (CGCGAATTCGCG)2 dodecamer (PDB ID: 1BNA) in order to predict the chosen binding site along with preferred orientation of the ligand inside the DNA minor groove.[30] The energetically most favourable conformation of the docked pose (Fig. 7–9) revealed that complexes **1** & **2** and the ligand bind to the minor groove of DNA, thereby slightly adjusting the DNA structure in such a way that a part of the planar phenyl ring makes favourable stacking interactions with DNA base pairs

and leads to van der Waals interactions with the DNA functional groups that define the stability of the groove. Moreover, two hydrogen bonding interactions with complexes **1** & **2** and three for the ligand in the minor groove have been predicted. The resulting relative binding energies of the docked structures for complexes **1**, **2** and the ligand were found to be −243.63, −212.42 and −202.02 kJ mol^{-1}, respectively. This indicates that a more potent binding between the DNA and complex **1** takes place than complex **2** and the ligand. This correlates well with the experimental DNA binding studies. Thus, the spectroscopic experimental results are harmonized with the molecular docking study as well.

3. Conclusion

The hydroxamato complexes of dioxomolybdenum and dioxotungsten have been designed, synthesised and structurally characterised using single crystal X-ray diffraction. The DNA binding studies using absorbance spectroscopy show that the intrinsic binding constants for complexes **1**, **2** and the ligand are found to be 5.2×10^4, 1.2×10^4 and 7.2×10^3 M^{-1} respectively. Furthermore, the Stern–Volmer quenching constant, K_{SV}, for complexes **1** and **2** is found to be 5.2×10^4 M^{-1} and 1.6×10^4 M^{-1} respectively. Both the complexes and the ligand exhibit effective protecting ability against radiation induced DNA damage. From the fluorometric assessment, 87% of the damaged DNA revives when the concentration of complex **1** is about 15 μM, whereas complex **2** and the ligand impart 80% and 72% protection respectively to damaged DNA at the same concentration. At a relatively higher concentration of the complex, about 95% of supercoiled plasmid (pUC19) DNA is protected. To establish the mechanism of protection by both complexes **1** and **2** as well as the ligand, radical scavenging experiments were performed which show that the Mo-complex (**1**) has a greater ability to scavenge free radicals compared to the W-complex (**2**) and the ligand. The EPR study on DPPH radical scavenging unequivocally supports the mechanism of protection by both complexes **1** and **2** and the ligand. The molecular docking study supports the binding of complexes **1** and **2** and the ligand to DNA where the relative binding energy of the lowest docked structure is found to be −243.63 kJ mol^{-1}, −212.42 kJ mol^{-1} and −202 kJ mol^{-1} for complexes **1** and **2** and the ligand respectively. Therefore, the present study realises the development of a metal based radioprotector and paves the way for the next phase trial with these molecules.

4. Experimental

4.1. Materials and physical methods

Molybdic acid ($MoO_3 \cdot 2H_2O$), tungstic acid and phenyl acetic acid were obtained from S.D. Fine Chem. (India). Hydroxylamine hydrochloride was of extra pure variety and was obtained from Merck (India). Potassium hydroxide pellets and methanol (G.R.) were products of Merck (India) and were used directly. DPPH (2,2-diphenyl-1-picrylhydrazyl), phenazine methosulfate (PMS), reduced nicotinamide adenine dinucleotide (NADH), nitroblue tetrazolium (NBT), quercetin, EDTA, mannitol and safranin were obtained from SRL, India. All other reagents used were of G.R. grade and were obtained from Merck (India). Analytical grade solvents used for physico-chemical studies were further purified by a literature method before use, wherever necessary. CT DNA and supercoiled plasmid pUC19 DNA were obtained from Sigma Chemical Company, USA, and Genei Bangalore, India, respectively.

4.2. Preparation of the ligand and the molybdenum and tungsten complexes

4.2.1. Synthesis of the ligand, *N*-(phenyl acetyl) hydroxamic acid (PAHH). The ligand was prepared using a literature method;[12] methyl phenylacetate was obtained by refluxing the mixture of phenylacetic acid, 13.6 g (0.1 mol), in 25 ml of dry methanol followed by addition of 1 ml of conc. H_2SO_4. Then to the above mixture, solid $NH_2OH \cdot HCl$, 14 g (0.2 mol), was added followed by the addition of a 25% methanolic KOH (0.4 mol) solution with constant stirring. The reaction mixture was neutralized with 1 N HCl solution, filtered off and the residue was washed with methanol. After the evaporation of this methanolic solution a white solid crystalline phenylacetyl hydroxamic acid was obtained. IR (KBr disc, cm^{-1}): 1634(s) (ν C═O), 1546(m) (ν C–N). ^1H NMR (CD_3OD, 300 MHz) δ in ppm: 4.8 (s, 1H, –OH), 3.44 (t, 2H, $–CH_2–$Ar), 7.226–7.312 (m, 5H, H-benzene ring), 5.46 (s, 1H, NH).

4.2.2. Synthesis of $[Mo(O)_2(PAH)_2]$ complex (1). $MoO_3 \cdot 2H_2O$ (0.45 g, 2.5 mmol) was dissolved in 5 ml of H_2O and then 0.5 ml (6.5 mmol) of 30% H_2O_2 was added to it with constant stirring at room temperature, which produced a pale yellow solution. Addition of a 20 ml methanolic solution of 0.742 g (5 mmol) phenyl acetyl hydroxamic acid (PAHH) to the above mixture under stirring conditions precipitated $[Mo(O)_2(PAH)_2]$ as a yellow solid. The solid was filtered off, washed thoroughly with water, methanol and diethyl ether, and then dried under vacuum. Single crystals (shiny yellow) suitable for X-ray diffraction were obtained by slow evaporation of the methanolic solution. Yield was 80%. Anal. calcd for $C_{16}H_{16}N_2O_6Mo$: C, 44.87; H, 3.7; N, 6.54; Mo, 22.40; Found. C, 44.94; H, 3.82; N, 6.59; Mo, 22.44; MS (EI): m/z 428.25; IR (KBr disc, cm^{-1}): 1597 (s) (ν C═O), 1498 (s) (ν C–N), 960 (s) & 905 (m) [ν Mo═O]. UV-vis; λ_{max} nm: 308(sh), 242(sh), 207. ^1H NMR (CD_3OD, 300 MHz) δ in ppm: 3.54 (s, 4H, $–CH_2–$Ar), 7.236–7.345 (m, 10H, H-benzene ring), 5.24 (s, 2H, NH).

4.2.3 Synthesis of $[W(O)_2(PAH)_2]$ complex (2). The $[W(O)_2(PAH)_2]$ complex was synthesized by the same procedure as described for the synthesis of complex **1**, only $WO_3 \cdot 2H_2O$, 0.65 g (2.5 mmol) was used instead of molybdic acid. Complex **2** as a cream coloured solid was separated out, filtered off, washed thoroughly with water, methanol and diethyl ether, and then dried under vacuum. Yield was 78%. The cream coloured single crystals suitable for X-ray

diffractometric studies were obtained by slow evaporation of the methanol solution. Anal. calcd for $C_{16}H_{16}N_2O_6W$: C, 53.69; H, 4.12; N, 9.4; W, 11.4; Found. C, 53.37; H, 4.22; N, 9.07; W, 10.97; MS (EI): *m*/*z* 516.15; IR (KBr disc, cm^{-1}): 1605 (s) (ν C═O), 1508 (s) (ν C–N), 967 & 915 (s) [ν W═O], 906 (m). UV-vis; λ_{max} nm; 312, 245(sh), 212. ^{1}H NMR (CD_3OD, 300 MHz) δ in ppm: 3.54 (s, 4H, $-CH_2-$Ar), 7.236–7.345 (m, 10H, H-benzene ring), 5.24 (s, 2H, NH).

4.3. X-Ray crystal structure determination

X-ray diffraction data for the crystals of complexes **1** and **2** were collected at 296 K on a Bruker AXS SMART APEX II diffractometer equipped with a CCD detector[31] with a fine focus of a 1.75 kW sealed tube using Mo Kα radiation (λ = 0.71073 Å). Crystallographic data and details of structure determination are summarized in Table 1. The data were processed using SAINT, and absorption corrections were made using SADABS.[32] The structure was solved by direct methods and refined by full-matrix least-squares on the basis of F^2 using the WINGX software, using the SHELX suites.[33] The non-hydrogen atoms were refined anisotropically, while the hydrogen atoms were placed geometrically (0.97 Å for $-CH_2$ group, 0.86 Å for N–H and 0.93 Å for aromatic C–H distance for different parent atoms) and refined using a riding model with isotropic displacements fixed (with a value equal to $1.2U_{eq}$ of its parent atoms). Perspective views of the molecules were obtained using ORTEP.[34]

4.4. DNA binding studies

4.4.1. UV-vis spectral study. The solutions of CT DNA in Tris-HCl/NaCl (50 mM Tris-HCl and 50 mM NaCl, pH 7.2) buffer medium gave a ratio of A_{260}/A_{280} of *ca.* 1.8–1.85, indicating that the DNA was sufficiently free from protein contamination. The DNA concentration per nucleotide was determined by absorption spectroscopy using the molar absorption coefficient at 260 nm. Stock solutions were stored at 4 °C and used within 4 days.

UV-vis spectra were recorded on a Shimadzu UV-1700 spectrophotometer. The electronic spectra of the complexes and the ligand were monitored in the presence and absence of DNA. In this absorption titration experiment, a fixed concentration of either complex **1** or **2** or the ligand was titrated with increasing amounts of DNA over a range of 10–150 μM in appropriate cases. To eliminate the absorbance of DNA, equal amounts of DNA were added to the reference solution as well. The intrinsic binding constant was determined using eqn (1):[35]

$$[\mathrm{DNA}]/(\varepsilon_a - \varepsilon_f) = [\mathrm{DNA}]/(\varepsilon_b - \varepsilon_f) + 1/[K_b(\varepsilon_b - \varepsilon_f)] \quad (1)$$

Here, [DNA] is the concentration of DNA in base pairs, the apparent absorption coefficients ε_a, ε_f and ε_b correspond to A_{obsd}/[complex], the extinction coefficient for the free complex, and the extinction coefficient for the complex in the fully bound form, respectively. Plots of $[\mathrm{DNA}]/(\varepsilon_a - \varepsilon_f)$ *versus* [DNA] gave a slope $1/(\varepsilon_b - \varepsilon_f)$ with *Y*-intercept $1/[K_b\ (\varepsilon_b - \varepsilon_f)]$. The intrinsic binding constant K_b was obtained from the ratio of the slope to the intercept.

4.4.2. Luminescence titrations. The excitation of the methanolic solution of complex **1** at 250 nm gives emission maxima at 307.5 nm while the excitation of complex **2** at 270 nm shows emission with λ_{max} 290 nm. For fluorescence titration experiments, the concentrations of complexes **1** and **2** were so adjusted that the final concentration of the test sample was 0.70 μM. This was titrated with increasing concentrations of DNA over the range 0–200 μM. The titration procedure was similar to that outlined above for spectrophotometric titrations. For all measurements, the samples were excited at 250 nm (complex **1**) and at 270 nm (complex **2**) and a similar slit width (10/10) was used.

The fluorescence quenching experimental data were further analysed using the Stern–Volmer equation:[36]

$$I_0/I = 1 + K_{SV}\ [\mathrm{DNA}] \quad (2)$$

where I_0 and I are the fluorescence intensities in the absence and presence of DNA, respectively; and K_{SV} is the Stern–Volmer quenching constant, which is a measure of the efficiency of quenching by DNA. The fluorescence titration data were also used to determine the binding constant of complexes with DNA. The concentration of the free drug was calculated according to eqn (3):[19]

$$C_F = C_T\ (I/I_0 - P)/(1 - P) \quad (3)$$

where C_T is the concentration of the drug added, C_F is the concentration of the free drug, and P is the ratio of the observed quantum yield of the fluorescence of the totally bound drug to that of the free drug. The value of P is obtained from a plot of I/I_0 *versus* 1/[DNA] such that it is the limiting fluorescence yield given by the *y* intercept. The amount of bound drug (C_B) at any concentration is equal to C_T–C_F.

A plot of r/C_F *versus* r, where r is equal to C_B/[DNA], was done by the modified Scatchard equation to understand the detailed binding pattern with binding sites:[16,19]

$$2r/C_f = K_b(1 - nr)[(1 - nr)/\{1 - (n - 1)r\}]^{n-1} \quad (4)$$

where K_b represents the intrinsic binding constant of the complex with DNA and n is the size of binding sites in base pairs.

4.4.3. Viscometric study. The viscosity of sonicated DNA[16,17,37] (average molecular weight of ~200 base pairs was measured using a Labsonic 2000 sonicator) was measured by a fabricated micro viscometer, maintained at 28 (±0.5) °C in a thermostatic water bath. The viscosities of the CTDNA, CTDNA-ligand, CTDNA-complex **1** and CTDNA-complex **2** were measured. Data were presented as $(\eta/\eta_o)^{1/3}$ *versus* the ratio of the concentration of either the ligand or complex **1** or **2** to that of the CT DNA, where η_o is the viscosity of CT DNA solution alone and η is the viscosity of CT DNA solution in the presence of either the complexes or the ligand. Viscosity values were calculated from the observed flow time of CT DNA

by the relation $\eta = t - t_0$, where t and t_0 are the values of flow times for the solution and the buffer respectively.

4.5. DNA damage and protection

4.5.1. Gamma irradiation. Gamma radiation was passed through DNA solution with the help of a GC-900 Gama Chamber, 2 Killo Courie. The CTDNA and DNA-complex samples were incubated at 37 °C for 30 min before irradiation; the incubated samples were then irradiated in a ^{60}Co γ-chamber at a dose rate of 69.3 Gy min^{-1} for a total dose of 3.068 kGy. For plasmid DNA samples the irradiation doses of 20 & 25 Gy were used.

4.5.2. Exposure to gamma-radiation and assessment of DNA damage

4.5.2.1. Estimation of radiation induced damage in CTDNA by fluorescence spectroscopy. Emission intensity measurements were carried out using a Perkin Elmer LS-55 spectroflourimeter. The radiation induced CTDNA damage was assessed by fluorescence spectroscopy using ethidium bromide (EB) bound CTDNA solution in Tris-HCl/NaCl buffer (pH 7.2). In this binding experiment, CTDNA solution was irradiated by a ^{60}Co-γ source as described earlier. Thereafter, this irradiated DNA was allowed to bind with EB, and the emission spectra were recorded at 591 nm after excitation at 500 nm (with excitation and emission slits 10 nm). This was compared with the fluorescence of the non-irradiated DNA-EB system under the identical experimental set-up.

The dose–response relation is obtained from the plot of $(I - I_a)/(I_0 - I_a)$ *versus* dose, where I_a is the fluorescence intensity of EB, I_0 is the fluorescence intensity of the unirradiated EB-DNA control and I is the fluorescence intensity of the irradiated EB-DNA sample.

4.5.2.2. Estimation of the protection from radiation induced DNA damage by the complexes and the ligand by fluorescence spectroscopy. CT DNA was pretreated with either the complex **1** or **2** or the ligand and was incubated for 30 min at 37 °C and then irradiated by a ^{60}Co-γ source at a dose rate of 69.3 Gy min^{-1} for 1 hour. These irradiated DNA solutions were allowed to bind with EB, and then the emission intensity at 591 nm was monitored. The solutions were excited at 500 nm (with excitation and emission slits 10 nm).

4.5.2.3. Protection from radiation induced plasmid pUC19 DNA damage by different concentrations of complexes and the ligand against different doses of gamma-radiation. The DNA damage protective ability of complexes **1** and **2** or the ligand was monitored by the agarose gel electrophoresis technique wherein the supercoiled pUC19 DNA (0.5 μg per reaction) solutions preincubated for 30 min with different concentrations of either complex **1**, **2** or the ligand [(0–2 mM) diluted with the Tris-HCl buffer to a total volume of 15 μl] were exposed to different doses, *e.g.* 20 and 25 Gy, of gamma radiation. After irradiation, they were mixed with loading buffer containing 25% bromophenol blue, 30% glycerol (3 μl) and finally loaded on 0.9% agarose gel. Electrophoresis was carried out at 80 V for 3 h in TAE buffer (Tris, acetic acid, and 1 mM EDTA, pH 7.2). The gel was stained using a 1.0 μg ml^{-1} ethidium bromide solution. Bands were visualized by UV light and photographed using the UVP BIO-DOC-IT Gel Documentation System. The extent of supercoiled (SC) pUC19 DNA damage induced by radiation and protection induced by the ligand and complexes was determined by analysing the intensities of the bands using UVP – BIO-DOC-IT LS Software.

4.6. Mechanism of protection from radiation induced DNA damage by the ligand and the complexes

4.6.1. Hydroxyl radical scavenging experiment. Hydroxyl radicals were generated in aqueous media through the Fenton-type reaction. Aliquots of 1.0 ml of 0.10 mmol aqueous safranin, 1 ml of 1.0 mmol aqueous EDTA-Fe(II), 1 ml of 3% aqueous H_2O_2, and different concentrations of either the ligand or complexes **1** and **2** were added to constitute the reaction mixture (3 ml). Samples without either the ligand or complexes **1** and **2** were used as the control in appropriate cases. The reaction mixtures were incubated at 37 °C for 30 min and the absorbances were then measured at 520 nm. All the tests were run in triplicate and results are expressed as the mean ± standard deviation (SD).[38] The scavenging effect for OH$^{\bullet}$ was calculated from the following expression:

$$\text{Scavenging ratio } (\%) = [(A_i - A_0)/(A_c - A_0)] \times 100\% \quad (5)$$

where A_i = absorbance in the presence of the test compound; A_0 = absorbance of the blank in the absence of the test compound; A_c = absorbance in the absence of the test compound, EDTA-Fe(II) and H_2O_2.

4.6.2. Superoxide radical scavenging experiment. The superoxide radical scavenging assay was based on the ability of the complex and the ligand to inhibit purple formazan formation by scavenging the superoxide radicals generated in a non-enzymatic phenazine methosulfate–nicotinamide adenine dinucleotide (PMS/NADH)–nitroblue tetrazolium (NBT) system.[39] Each 3 ml reaction mixture contained 20 mM phosphate buffer (pH 7.4), 20 mM of NADH, 0.45 mM PMS, 0.15 mM of NBT and various concentrations of either the ligand, complex **1** or complex **2**. The above mixtures were incubated for 5 min at 37 °C, and then absorbance was measured at 560 nm against an appropriate blank to determine the quantity of formazan generated.

All the tests were run in triplicate and results are expressed as mean ± standard deviation (SD). The scavenging effect for superoxide anion radicals was calculated using eqn (5).

4.6.3. DPPH radical scavenging activity

4.6.3.1. DPPH radical scavenging activity by EPR spectroscopy. Electron paramagnetic resonance (EPR) measurements were performed at room temperature (298 K) on a Jeol JES-FA 200 ESR spectrometer equipped with a Jeol microwave bridge. The spectroscopic parameters were: frequency 9.44 GHz, field sweep 100 mT, microwave power 0.998 mW, and modulation amplitude 3000 mT and EPR were measured in a Jeol Quartz pyrex EPR tube, no. 193 5D. The stability of freshly prepared methanol solution of DPPH was monitored[40] for 30 min, and no significant loss of signal was detected. Stock solutions of complexes **1** and **2** or the ligand and

DPPH were prepared in methanol. In 60 mM DPPH solution, different concentrations (0–60 mM) of either complexes **1** & **2** or the ligand were added and mixed thoroughly. The EPR signal was recorded 2 minutes after mixing either the complexes or the ligand in appropriate cases with the DPPH solution under identical instrumental conditions.

4.6.3.2. DPPH radical scavenging activity by electronic absorbance spectroscopy. The 2,2-diphenyl-1-picrylhydrazyl (DPPH) radical scavenging activity of the compounds was measured according to the Blois method.[41,42] The DPPH radical is a stable free radical. Because of the odd electron, DPPH shows a strong absorption band at 517 nm in the visible spectrum. The absorption decreases as the odd electron becomes paired off in the presence of a free radical scavenger. Different concentrations of the ligand, complexes **1** & **2** were added to a solution of DPPH in methanol (0.1 μM, 3 ml), and the final volume was made with triple distilled water. The solution was incubated at 37 °C for 30 min in the dark. All the tests were run in triplicate and results are expressed as mean ± standard deviation (SD). The scavenging effect for DPPH radicals was calculated using eqn (5).

4.7. Molecular docking

The rigid molecular docking studies were performed using HEX 6.3[43] software (http://www.loria.fr/~ritchied/hex/). For the docking study, the structure of the ligand was generated from the PRODRG 2 server.[44] The geometry of the ligand was optimized by applying the CHARMm force field in Discovery studio 3.1, and the coordinates of metal complexes **1** and **2** were taken from its crystal structure as a CIF file and was converted to the PDB format using Mercury software (http://www.ccdc.cam.ac.uk/). The crystal structure of the B-DNA dodecamer $d(CGCGAATTCGCG)_2$ (PDB ID: 1BNA) was downloaded from the Protein Data Bank (http://www.rcsb.org./pdb). All calculations were carried out on an Intel I5, 3.1 GHz based machine with MS Windows 7 as the operating system. Visualization of the docked pose was done using Discovery studio 3.1 and the PyMol (http://pymol.sourceforget.net/) molecular graphics program.

Acknowledgements

The authors are thankful to UGC-DAE-CSR-KC for financial support in the form of a major research project to KKM [UGC-DAE-CSR-KC/CRS/09/RC-03/]. The single crystal X-ray diffractometer, EPR, and NMR spectrometers used in this work have been funded by the Department of Science and Technology (DST-FIST, Department of Chemistry, J.U.), New Delhi, India, and the Circular Dichroism spectrometer has been funded by UGC-CAS, to the Department of Chemistry, J.U. The authors are thankful to UGC, New Delhi for funding the UVP Bio Doc-IT GEL Imaging system in the form of a major research project to KKM [39-706/2010(SR)]. The authors extend their thanks to Dr A Dutta of UGC, DAE CSR, KC for assisting in running the GC 900 gamma radiation equipment.

References

1 (*a*) U. Ringborg, D. Bergqvist and B. Brorsson, *Acta Oncol.*, 2003, **42**, 357–375; (*b*) E. J. Hall and A. J. Giaccia, *Radiobiology for the Radiologist*, Lippincott Williams & Wilkins, Philadelphia, 6th edn, 2006, p. 546.

2 (*a*) M. Karbownik and R. Reiter, *Exp. Biol. Med.*, 2000, **225**, 9–22; (*b*) C. Von Sonntag, *The Chemical Basis of Radiation Biology*, Taylor & Francis, London, 1987, vol. 31, pp. 116–166 & 221–294.

3 (*a*) D. Q. Brown, J. W. Pittock III and J. S. Rubinstein, *Int. J. Radiat. Oncol., Biol., Phys.*, 1982, **8**, 565–570; (*b*) D. R. Cassatt, C. A. Fazenbaker, C. M. Bachy and M. S. Hanson, *Semin. Radiat. Oncol.*, 2002, **12**, 97–102.

4 (*a*) M. H. Whitnall, T. B. Elliotta, R. A. Hardinga, C. E. Inala, M. R. Landauera, C. L. Wilhelmsena, L. McKinneya, V. L. Minera, W. E. Jackson IIIa, R. M. Loriab, G. D. Ledneya and T. M. Seeda, *Int. J. Immunopharmacol.*, 2000, **22**, 1–14; (*b*) M. R. Landauer, V. Srinivasan and T. M. Seed, *J. Appl. Toxicol.*, 2003, **23**, 379–385.

5 (*a*) M. Koukourakis, *J. Clin. Oncol.*, 2000, **18**, 2226–2233; (*b*) D. M. Brizel and J. Overgaard, *Lancet Oncol.*, 2003, **4**, 378–381; (*c*) L. Cai, G. Tsiapalis and M. G. Cherian, *Chem. Biol. Interact.*, 1998, **115**, 141–151.

6 (*a*) S. J. Hosseinimehr, S. Emami, S. Mohammad Taghdisi and S. Akhlaghpoor, *Eur. J. Med. Chem.*, 2008, **43**, 557–561; (*b*) M. Tanaka, K. Ohkubo and S. Fukuzumi, *J. Am. Chem. Soc.*, 2006, **128**, 12372–12373.

7 (*a*) V. Brabec, J. Malina, N. Margiotta, G. Natile and J. Kasparkova, *Chem.–Eur. J.*, 2012, **18**, 15439–15448; (*b*) J. C. Joyner, J. Reichfield and J. A. Cowan, *J. Am. Chem. Soc.*, 2011, **39**, 15613–15626; (*c*) J. C. Joyner, K. D. Keuper and J. A. Cowan, *Dalton Trans.*, 2012, **41**, 6567–6578; (*d*) É. A. Enyedy, É. Sija, T. Jakusch, C. G. Hartinger, W. Kandioller, B. K. Keppler and T. Kiss, *J. Inorg. Biochem.*, 2013, **127**, 161–168.

8 (*a*) G. Moula, M. Bose and S. Sarkar, *Inorg. Chem.*, 2013, **52**, 5316–5327; (*b*) J. Mitra and S. Sarkar, *Dalton Trans.*, 2013, **42**, 3050–3058; (*c*) A. Majumdar and S. Sarkar, *Coord. Chem. Rev.*, 2011, **255**, 1039–1054; (*d*) P. K. Chaudhury, S. K. Das and S. Sarkar, *J. Biochem.*, 1996, **319**, 953–959; (*e*) S. K. Das, P. K. Chaudhury, D. Biswas and S. Sarkar, *J. Am. Chem. Soc.*, 1994, **116**, 9061–9070; (*f*) B. E. Schultz, S. F. Gheller, M. C. Muetterties, M. J. Scott and R. H. Holm, *J. Am. Chem. Soc.*, 1993, **115**, 2714–2722.

9 (*a*) N. P. L'vov, A. N. Nosikov and A. N. Antipov, *Biochemistry*, 2002, **67**, 196–200; (*b*) K. V. Rajagopalan, *Annu. Rev. Nutr.*, 1998, **8**, 401–427; (*c*) M. P. Coughlan, *J. Inherit. Metab. Dis.*, 1983, **6**, 70–77; (*d*) L. G. Ljungdahe, *Trends Biochem. Sci.*, 1976, **1**, 63–65; (*e*) B. Fischer, J. H. Enemark and P. Basu, *J. Inorg. Biochem.*, 1998, **72**, 13–21.

10 (*a*) J. B. Neilands, *Struct. Bonding*, 1984, **58**, 1–24; (*b*) K. N. Raymond and C. J. Carrano, *Acc. Chem. Res.*, 1979, **12**, 183–185; (*c*) S. Belvedere, D. J. Witter, J. Yan, J. P. Secrist, V. Richon and T. A. Miller, *Bioorg. Med. Chem. Lett.*, 2007, **17**, 3969–3971.

11 (*a*) M. Z. Koncic, Z. Rajic, N. Petric and B. Zorc, *Acta. Pharm.*, 2009, **59**, 234–242; (*b*) Y. Zhang, H. Fang, J. Feng, Y. Jia, X. Wang and W. Xu, *Eur. J. Med. Chem.*, 2011, **54**, 5532–5539.
12 A. K. Majumdar, *N-Benzoylphenyl Hydroxylamine and its Analogues*, ed. R. Belcher and A. Frieser, Pergamon Press, Braunschweig, 1971.
13 (*a*) H. Oku, N. Ueyama and A. Nakamura, *Inorg. Chem.*, 1995, **34**, 3667–3676; (*b*) A. A. Eagle, E. R. T. Tiekink and C. G. Young, *Inorg. Chem.*, 1997, **36**, 6315–6322.
14 (*a*) S. M. O. Quintal, H. I. S. Nogueira, H. M. Carapuça, V. Félix and M. G. B. Drew, *J. Chem. Soc., Dalton Trans.*, 2001, 3196–3201; (*b*) J. H. Enemark and C. G. Young, *Adv. Inorg. Chem.*, 1993, **40**, 1–88; (*c*) M. G. B. Drew and I. B. Tomkins, *Acta Crystallogr., Sect. B: Struct. Crystallogr. Cryst. Chem.*, 1970, **26**, 1161–1165.
15 (*a*) T. K. Si, S. S. Paul, M. G. B. Drew and K. K. Mukherjea, *Dalton Trans.*, 2012, **41**, 5805–5815; (*b*) H. R. Holm, *Chem. Rev.*, 1987, **87**, 1401–1449.
16 (*a*) S. Patra, S. Chatterjee, T. K. Si and K. K. Mukherjea, *Dalton Trans.*, 2013, **42**, 13425–13435; (*b*) S. Pacigová, R. Gyepes, J. Tatierskya and M. Sivák, *Dalton Trans.*, 2008, 121–130; (*c*) S. Liu, H. Zhu and J. Zubieta, *Polyhedron*, 1989, **8**, 2473–2480.
17 (*a*) D. V. Partyka, R. J. Staples and R. H. Holm, *Inorg. Chem.*, 2003, **42**, 7877–7886; (*b*) R. Lai, V. Piasco, C. Berlin, C. Ross, J. Feneau-Dupont and J. P. Declercq, *Polyhedron*, 1993, **12**, 2513–2517.
18 (*a*) K. R. Barnard, M. Bruck, S. Huber, C. Grittini, J. H. Enemark, R. W. Gable and A. G. Wedd, *Inorg. Chem.*, 1997, **36**, 637–649; (*b*) F. Han, N. Taulier and T. V. Chalikian, *Biochemistry*, 2005, **44**, 9785–9794; (*c*) P. E. Pjura, K. Grzeskowiak and R. E. Dickerson, *J. Mol. Biol.*, 1987, **197**, 257–271.
19 (*a*) J. D. McGhee and P. H. Von Hippel, *J. Mol. Biol.*, 1974, **86**, 469–489; (*b*) J. R. Lakowicz and G. Weber, *Biochemistry*, 1973, **12**, 4161–4170.
20 S. Satyanarayana, J. C. Dabrowiak and J. B. Chaires, *Biochemistry*, 1992, **31**, 9319–9324.
21 (*a*) J. B. Chaires, *Biopolymers*, 1998, **44**, 201–215; (*b*) P. Arya and B. Willis, *J. Am. Chem. Soc.*, 2003, **125**, 12398–12399.
22 (*a*) E. Froehlich, J. S. Mandeville, C. M. Weinert, L. Kreplak and H. A. Tajmir-Riahi, *Biomacromolecules*, 2011, **12**, 511–517; (*b*) K. R. Rogers, A. Apostol, S. J. Madsen and C. W. Spencer, *Anal. Chem.*, 1999, **71**, 4423–4426; (*c*) S. S. Kumar, R. C. Chaubey, T. P. A. Devasagayam, K. I. Priyadarshini and P. S. Chauhan, *Mutat. Res.*, 1999, **425**, 71–79.
23 C. K. Nair and V. P. Salvi, *Mutat. Res.*, 2008, **650**, 48–54.
24 I. B. Afanasev, E. A. Ostrakhovitch, E. V. Mikhallchi, G. A. Ibragimova and L. G. Korkina, *Biochem. Pharmacol.*, 2001, **61**, 677–684.
25 F. V. Botelho, J. I. Alvarez-Leite, V. S. Lemos, A. M. C. Pimenta, H. D. R. Calado, T. Matencio, C. T. Miranda and E. C. Pereira-Maia, *J. Inorg. Biochem.*, 2007, **101**, 935–943.
26 Z. Gao, K. Huang, X. Yang and H. Xu, *Biochim. Biophys. Acta*, 1999, **1472**, 643–650.
27 M. C. Foti, C. Daquino and C. Geraci, *J. Org. Chem.*, 2004, **69**, 2309–2314.
28 (*a*) Q. Wang, Z. Y. Yang, G. F. Qi and D. D. Qin, *Eur. J. Med. Chem.*, 2009, **44**, 2425–2433; (*b*) C. Beauchamp and I. Fridovich, *Anal. Biochem.*, 1971, **44**, 276–287.
29 (*a*) T. R. Li, Z. Y. Yang, B. D. Wang and D. D. Qin, *Eur. J. Med. Chem.*, 2008, **43**, 1688–1695; (*b*) J. I. Ueda, N. Saito, Y. Shimazu and T. Ozawa, *Arch. Biochem. Biophys.*, 1996, **333**, 377–384.
30 (*a*) R. Rohs, I. Bloch, H. Sklenar and Z. Shakked, *Nucleic Acids Res.*, 2005, **33**, 7048–7057; (*b*) R. Filosa, A. Peduto, S. Di Micco, P. de Caprariis, M. Festa, A. Petrella, G. Capranico and G. Bifulco, *Bioorg. Med. Chem.*, 2009, **17**, 13–24; (*c*) R. Corradini, S. Sforza, T. Tedeschi and R. Marchelli, *Chirality*, 2007, **19**, 269–294; (*d*) B. K. Sahoo, K. S. Ghosh, R. Bera and S. Dasgupta, *Chem. Phys.*, 2008, **351**, 163–169.
31 Bruker, *APEX 2, SAINT, XPREP*, Bruker AXS Inc., Madison, Wisconsin, USA, 2007.
32 Bruker, *SADABS*, Bruker AXS Inc., Madison, Wisconsin, USA, 2001.
33 SHELXS 97 and SHELXL 97: G. M. Sheldrick, *Acta Crystallogr., Sect. A: Found. Crystallogr.*, 2008, **64**, 112–122.
34 L. J. Farrugia, Ortep-3 for Windows, *J. Appl. Crystallogr.*, 1997, **30**, 565–566.
35 (*a*) M. Selim, S. R. Choudhary and K. K. Mukherjea, *Int. J. Biol. Macromol.*, 2007, **41**, 579–583; (*b*) R. K. Tubbs, W. E. Ditmars Jr. and Q. Van Winkle, *J. Mol. Biol.*, 1964, **9**, 545–557.
36 (*a*) M. Selim and K. K. Mukherjea, *J. Biomol. Struct. Dyn.*, 2009, **26**, 561–566; (*b*) A. Wolfe, G. H. Shimer and T. Meehan, *Biochemistry*, 1987, **26**, 6392–6396.
37 (*a*) J. B. Chaires, N. Dattagupta and D. M. Crothers, *Biochemistry*, 1982, **21**, 3933–3940; (*b*) S. R. Chowdhury, M. Selim, S. Chatterjee, S. Igarashi, Y. Yukawa and K. K. Mukherjea, *J. Coord. Chem.*, 2012, **65**, 3469–3480.
38 (*a*) T. Nash, *Biochem. J.*, 1953, **55**, 416–421; (*b*) E. Kunchandy and M. N. A. Rao, *Int. J. Pharm.*, 1990, **58**, 237–240.
39 (*a*) C. Beauchamp and I. Fridovich, *Anal. Biochem.*, 1971, **44**, 276–287; (*b*) M. Fontana, L. Mosca and M. A. Rosei, *Biochem. Pharmacol.*, 2001, **61**, 1253–1257; (*c*) Y. Jin and J. A. Cowan, *J. Am. Chem. Soc.*, 2005, **127**, 8408–8415; (*d*) A. Samuni, S. Goldstein, A. Russo, J. B. Mitchell, M. C. Krishna and P. Neta, *J. Am. Chem. Soc.*, 2002, **124**, 8719–8724.
40 (*a*) T. Hatano, H. Kagawa, T. Yasuhara and T. Okuda, *Chem. Pharm. Bull.*, 1988, **36**, 2090–2097; (*b*) J. A. Weil, J. R. Bolton and J. E. Wertz, *Electron paramagnetic resonance: Elementary theory and applications*, New York, John Wiley & Sons, 1994.
41 M. S. Blois, *Nature*, 1958, **181**, 1199–1200.
42 H.-M. Kang and M. E. Saltveit, *J. Agric. Food Chem.*, 2002, **50**, 513–518.
43 D. Mustard and D. W. Ritchie, *Struct. Funct. Bioinf.*, 2005, **60**, 269–272.
44 A. W. Schuttelkopf and D. M. F. Van Aalten, *Acta crystallogr., Sect. D: Biol. Crystallogr.*, 2004, **60**, 1355–1363.

